












# High-fidelity Imaging of the Inner AU Mic Debris Disk: Evidence of Differential Wind Sculpting?

John P. Wisniewski<sup>1</sup> , Adam F. Kowalski<sup>2,3</sup> , James R. A. Davenport<sup>4</sup> , Glenn Schneider<sup>5</sup> , Carol A. Grady<sup>6</sup>, Leslie Hebb<sup>7</sup> , Kellen D. Lawson<sup>1</sup>, Jean-Charles Augereau<sup>8</sup>, Anthony Boccaletti<sup>9</sup>, Alexander Brown<sup>10</sup>, John H. Debes<sup>11</sup> , Andras Gaspar<sup>5</sup> , Thomas K. Henning<sup>12</sup>, Dean C. Hines<sup>11</sup> , Marc J. Kuchner<sup>13</sup>, Anne-Marie Lagrange<sup>14</sup>, Julien Milli<sup>15</sup> , Elie Sezestre<sup>8</sup>, Christopher C. Stark<sup>11</sup>, and Christian Thalmann<sup>16</sup>

<sup>1</sup> Homer L. Dodge Department of Physics and Astronomy, University of Oklahoma, 440 West Brooks Street, Norman, OK 73019, USA; [wisniewski@ou.edu](mailto:wisniewski@ou.edu)

<sup>2</sup> Department of Astrophysical and Planetary Sciences, University of Colorado Boulder, 2000 Colorado Avenue, Boulder, CO 80305, USA

<sup>3</sup> National Solar Observatory, University of Colorado Boulder, 3665 Discovery Drive, Boulder, CO 80303, USA

<sup>4</sup> Department of Astronomy, University of Washington, Seattle, WA 98195, USA

<sup>5</sup> Steward Observatory and the Department of Astronomy, The University of Arizona, 933 North Cherry Avenue, Tucson, AZ 85721, USA

<sup>6</sup> Eureka Scientific, 2452 Delmer, Suite 100, Oakland, CA 96002, USA

<sup>7</sup> Department of Physics, Hobart and William Smith Colleges, 300 Pulteney Street, Geneva, NY 14456, USA

<sup>8</sup> Univ. Grenoble Alpes, CNRS, IPAG, F-38000 Grenoble, France

<sup>9</sup> LESIA, Observatoire de Paris, Université PSL, CNRS, Sorbonne Université, Univ. Paris Diderot, Sorbonne Paris Cité, 5 Place Jules Janssen, F-92195 Meudon, France

<sup>10</sup> Center for Astrophysics and Space Astronomy, 389 UCB, University of Colorado, Boulder, CO 80309-0389, USA

<sup>11</sup> Space Telescope Science Institute, Baltimore, MD 21218, USA

<sup>12</sup> Max-Planck-Institut für Astronomie, Königstuhl 17, D-69117 Heidelberg, Germany

<sup>13</sup> Exoplanets and Stellar Astrophysics Laboratory, NASA Goddard Space Flight Center, 8800 Greenbelt Road, Greenbelt, MD 20771, USA

<sup>14</sup> Université Grenoble Alpes, CNRS, IPAG, F-38000, Grenoble, France

<sup>15</sup> European Southern Observatory (ESO), Alonso de Córdova 3107, Vitacura, Casilla 19001, Santiago, Chile

<sup>16</sup> Eidgenössische Technische Hochschule, Zurich, Switzerland

Received 2019 July 23; revised 2019 August 26; accepted 2019 August 31; published 2019 September 18

## Abstract

We present new high-fidelity optical coronagraphic imagery of the inner  $\sim 50$  au of AU Mic’s edge-on debris disk using the BAR5 occulter of the *Hubble Space Telescope* Imaging Spectrograph (*HST*/STIS) obtained on 2018 July 26–27. This new imagery reveals that “feature A,” residing at a projected stellocentric separation of 14.2 au on the southeast side of the disk, exhibits an apparent “loop-like” morphology at the time of our observations. The loop has a projected width of 1.5 au and rises 2.3 au above the disk midplane. We also explored *Transiting Exoplanet Survey Satellite* photometric observations of AU Mic that are consistent with evidence of two starspot complexes in the system. The likely co-alignment of the stellar and disk rotational axes breaks degeneracies in detailed spot modeling, indicating that AU Mic’s projected magnetic field axis is offset from its rotational axis. We speculate that small grains in AU Mic’s disk could be sculpted by a time-dependent wind that is influenced by this offset magnetic field axis, analogous to co-rotating solar interaction regions that sculpt and influence the inner and outer regions of our own Heliosphere. Alternatively, if the observed spot modulation is indicative of a significant misalignment of the stellar and disk rotational axes, we suggest that the disk could still be sculpted by the differential equatorial versus polar wind that it sees with every stellar rotation.

*Unified Astronomy Thesaurus concepts:* [Debris disks \(363\)](#); [Circumstellar disks \(235\)](#); [Starspots \(1572\)](#); [M dwarf stars \(982\)](#)

## 1. Introduction

AU Mic is a nearby (9.8 pc; Gaia Collaboration et al. 2018), M1Ve star that is a member of the  $23 \pm 3$  Myr old  $\beta$  Pic moving group (Mamajek & Bell 2014). Since the discovery and early observations of the spatially resolved, edge-on debris disk associated with the system (Kalas et al. 2004; Liu 2004) that is gas poor (Roberge et al. 2005), subsequent high-contrast imaging has probed the structure of disk in scattered light from projected stellocentric radii of 10 au (Wang et al. 2015) to 210 au (Schneider et al. 2014), as well as distances in between (Krist et al. 2005; Metchev et al. 2005; Fitzgerald et al. 2007; Graham et al. 2007; Boccaletti et al. 2015, 2018). Along with longer wavelength mm observations, these data suggest that the general architecture of AU Mic’s debris system might be similar to the asteroid belt and

Kuiper Belt in our own solar system. AU Mic has a “birth ring” of material near 43 au that forms micron-sized particles from collisions between larger bodies (see e.g., Strubbe & Chiang 2006; Graham et al. 2007; MacGregor et al. 2013; Matthews et al. 2015), as well as an extended halo comprising approximately micron-sized grains (Matthews et al. 2015). While it has been suggested that the inner ( $<30$  au) disk is devoid of small, micron-sized grains (Strubbe & Chiang 2006), recent observations suggest at least some small grains still exist here (Lomax et al. 2018). Early searches for planets in the system yielded null results (Metchev et al. 2005; Hebb et al. 2007); however, Plavchan et al. (2019) presents the observational detection of the inner planetary population in the system.

AU Mic is particularly notable in that it is the first spatially resolved debris disk where dynamical processes in the disk are being resolved on  $<$ year timescales. Boccaletti et al. (2015) analyzed multi-epoch imagery of the disk and discovered at least five spatially resolved features on the southeast side of the disk that clearly change location as a function of time, with



Original content from this work may be used under the terms of the [Creative Commons Attribution 3.0 licence](#). Any further distribution of this work must maintain attribution to the author(s) and the title of the work, journal citation and DOI.

measured projected tangential speeds of some features indicating that they are moving on unbound, non-Keplerian trajectories. Follow-up studies have identified additional moving features on both the southeast and northwest sides of the disk, and revealed that these features also exhibit vertical (perpendicular to the disk midplane) motion (e.g., Boccaletti et al. 2018 and Grady et al. 2019). More recently, Lomax et al. (2018) noted a change in the color of the disk between 30 and 45 au from being increasingly bluer with stellocentric distance (Krist et al. 2005; Metchev et al. 2005; Fitzgerald et al. 2007) to a constant, smaller blue color, suggesting a reduction in the relative number of small grains at these stellocentric distances that could be causally correlated to the passage of fast-moving features seen in broadband scattered light imagery.

The mechanism(s) driving the observed variability in AU Mic’s debris disk remain hotly debated within the literature. Sezestre et al. (2017) suggested that the moving dust features are either generated by resonance with a parent body that orbits at  $8 \pm 2$  au or at a recent large collision that generated a large population of smaller bodies, which are then dispersed by the stellar wind. Chiang & Fung (2017) proposed that the moving features in AU Mic’s disk are caused by the interaction between the star’s wind and repeated “dust avalanche” events. These avalanches are triggered in a zone marked by the intersection of AU Mic’s primary debris ring and a proposed secondary ring of dust left behind by the catastrophic disruption of an object up to the size of the Kuiper Belt Object Varuna (radius 450 km; Lellouch et al. 2013). Both Chiang & Fung (2017) and Daley et al. (2019) discussed some of the potential challenges to this avalanche scenario. Chiang & Fung (2017) also predicted a vertical velocity component in moving features caused by the star’s magnetized wind exerting a Lorentz force on the dust grains, potentially regulated by the stellar magnetic activity cycle. These dynamical models assume significantly different wind properties: Sezestre et al. (2017) adopted a constant wind that induces a mass-loss rate that is  $50\times$  solar, whereas Chiang & Fung (2017) adopted a variable wind that induces a mass-loss rate that is  $500\times$ – $5000\times$  solar (see also Boccaletti et al. 2018). Augereau & Beust (2006) and Schüppler et al. (2015) detailed why AU Mic’s mass-loss rate is expected to be larger than that of the Sun, but this mass-loss rate has not been observationally confirmed (e.g., Wood et al. 2005). Sezestre et al. (2017) noted that these dramatically different mass-loss rates have profound impacts on the grain blowout sizes that would be in operation.

In this Letter, we present new white-light optical coronagraphic imagery of the inner region of AU Mic’s disk obtained with the *Hubble Space Telescope* Imaging Spectrograph (*HST*/STIS) in 2018 using the BAR5 occulter. We describe the acquisition and reduction of these data in Section 2. We highlight the new morphologies of AU Mic’s disk revealed by these data, including dramatic apparent loop-like structures seen in projection, in Section 3. We explore some of the potential mechanisms that could create these morphological features in the context of preliminary analysis of new constraints on the star’s activity as enabled by NASA/*Transiting Exoplanet Survey Satellite* (*TESS*) data in Section 4.

## 2. *HST* BAR5 Coronagraphic Imagery

Coronagraphic observations of AU Mic and associated point-spread function (PSF) template star HD 191849 were obtained with the *HST*/STIS BAR5 occulter, a  $0''.15$  wide

rectangular bar, in GO-15219 (PI: J. Wisniewski). The 50CORON imaging mode used provided an unfiltered spectral passband of pivot wavelength  $0.575 \mu\text{m}$  with  $\text{FWHM} = 0.433 \mu\text{m}$ , an image scale of  $50.77 \text{ mas pixel}^{-1}$ , and spatial resolution of  $\sim 72 \text{ mas}$ .

Observations of AU Mic were obtained in three sequential orbits on 2018 July 26–27 using a sub-array readout that sampled the inner  $2''.5$  (100 pixels) of the disk. The major axis of the disk was oriented approximately orthogonal to the long axis of the BAR5 occulter in the second orbit, and the telescope was rolled by  $\pm 6.5^\circ$  in the first and third orbits. Within each orbit, 20–21 images of 16.6 s duration were obtained at each of three cross-BAR5 dither positions offset by  $(-1/4, 0, +1/4)$  pixels orthogonally with respect to the midline of the occulter. HD 191849 was observed immediately thereafter using two sequential orbits, using the same cross-BAR5 dither technique, as a PSF reference. 22–26 images per dither location were obtained using 11.5 s per image integrations. We also obtained a single-orbit observation of AU Mic on 2018 September 22 with the disk aligned along the long axis of the BAR5 occulter, using the same dither and integration scheme described above. These disk-obscured images provide perfect color-matching to explore alternate methods to achieve better PSF subtraction.

These data were reduced and calibrated using the same procedures and techniques as outlined in Schneider et al. (2018). Following bias, dark, and flat-field correction using the temporally nearest calibration data, we located the position of the occulted star in each image using the “X marks the spot” diffraction spike fitting method of Schneider et al. (2014). Within each orbit, all images observed with the same dither position were then median combined and cleaned of cosmic-rays. Image co-registration, and later PSF subtractions, were done with sinc-apodized bi-cubic sub-pixel interpolation using the IDL-based, IDP3 software (Stobie & Ferro 2006). The relative brightness and  $(x, y)$  position of the PSF star HD 191849 were treated, and iteratively adjusted, as free parameters to minimize the variance in difference image pixels not dominated by disk flux.

We found that while chromatic residuals were fully mitigated with our disk-obscured BAR5 observation of AU Mic on 2018 September 22, using this orbit as a PSF template led to substantial PSF subtraction residuals caused by differential wavefront errors induced by the non-contemporaneous (e.g.,  $\sim 2$  month separation) observation from our three sequential orbits that resolved AU Mic’s disk. We therefore adopt and use our sequentially contemporaneous observations of HD 191849 as the PSF reference for our final disk imagery. Following PSF subtraction, our multi-roll images were re-oriented to a common orientation and median combined after masking known imaging artifacts.

## 3. Analysis

### 3.1. *HST* Imaging Results

We display our resultant PSF-subtracted imagery of AU Mic taken with STIS’ BAR5, after  $1/r^2$  intensity scaling, in panels (b)–(d) of Figure 1, along with 2017-epoch WedgeA0.6 imagery of the inner disk from Grady et al. (2019) in panel a. The superlative sub-pixel dithering of our BAR5 data provide an enhanced view of the morphology of feature A in the disk, compared to 2017-epoch WedgeA0.6 data. In particular, Figure 1 (panels (b)–(c)) and Figure 2 reveal that feature A has a distinctive “loop-like” appearance. It is not

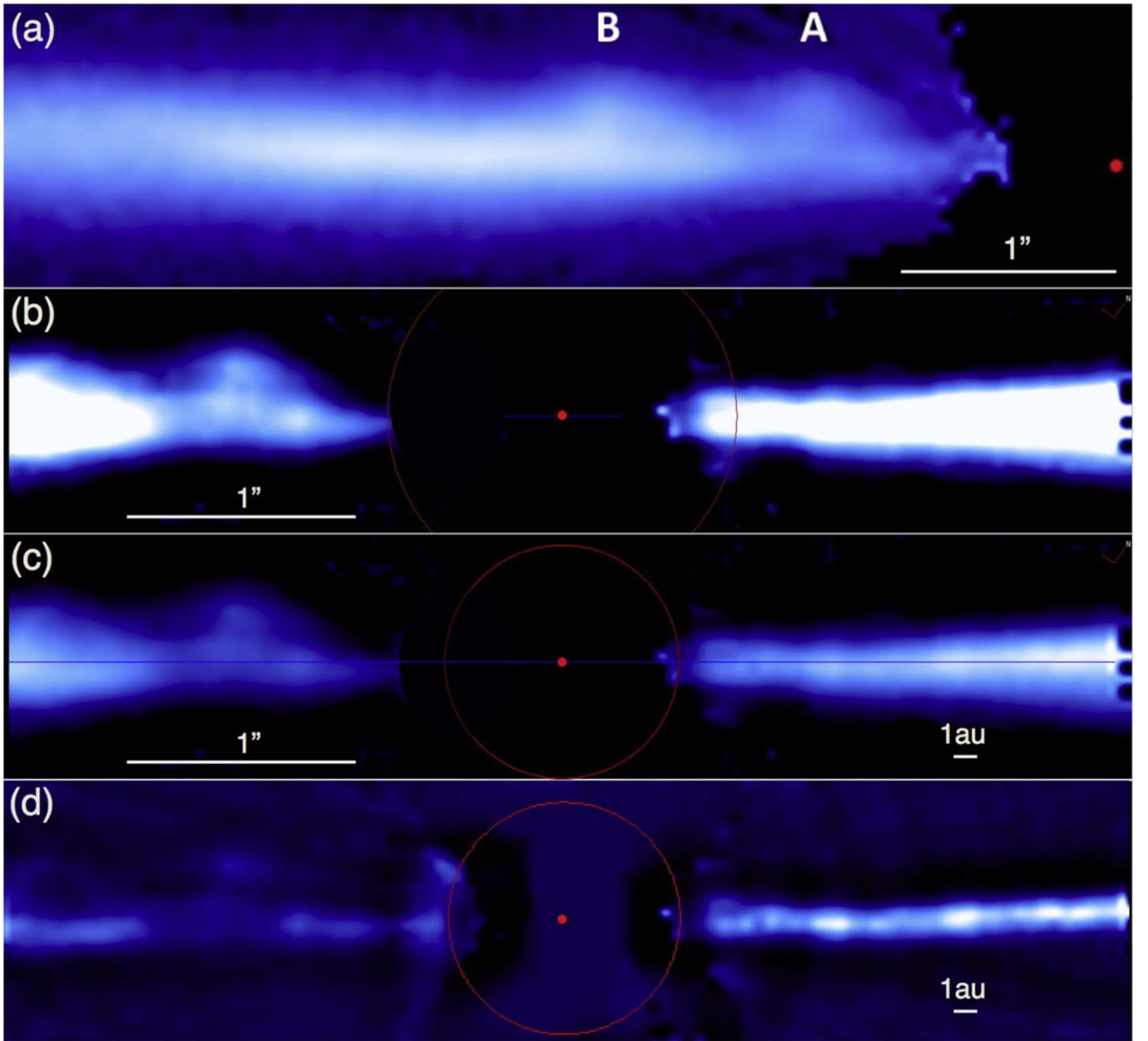


**Figure 1.** Inner  $5''/2$  (50 au) region of the southeast side of the AU Mic disk from *HST*/STIS WedgeA0.6 imaging of the system in 2017 is shown in panel (a), as adopted from Grady et al. (2019). These data have been scaled by  $1/r^2$  and are displayed using a log scale optimized to emphasize the out-of-plane features A and B. Panels (b) and (c) depict *HST*/STIS BAR5 observations presented in this study, also scaled by  $1/r^2$ . The field of view (FOV) in both of these panels is  $4''93 \times 1''02$ , and the location of the central star is depicted by a red dot. Panels (b) and (c) adopted differently stretched log-based intensity scales to emphasize the dramatic “loop-like” morphology that feature A exhibits. Applying a high-pass filter to the BAR5 data (panel d) enhances the visibility of disk substructure seen on au scales.

possible to determine whether the “loop-like” morphology of feature A remains coherent as the feature moves within the disk, due to the single-epoch nature of these high-resolution data. As feature A is moving radially at  $\sim 1.7$  STIS pixels  $\text{yr}^{-1}$  (i.e.,  $\sim 1.2$  resolution elements  $\text{yr}^{-1}$ ; Grady 2019), annual observations are commensurate with resolvable motions of this substructure. *HST* GO-15907 is pursuing these observations and could enable discrimination of the potential role of projection. Moreover, a larger portion of the disk will be read out in these planned observations, allowing us to determine whether or not other known moving features in the disk exhibit loop-like morphologies that are similar to that found for feature A.

To further explore new information encoded within these high-resolution BAR5 imagery, we applied a high-pass filter to these data (panel (d), Figure 1). We fit two one-dimensional Gaussians to the loop-like structure to quantify its size and projected location. These fits reveal that the loop-like structure has a projected width of 1.5 au and rises to a projected height above the midplane of 2.3 au. The centroid of these fits also imply that the loop-like structure resides at a projected stellocentric radial distance of 14.2 au from the host star.



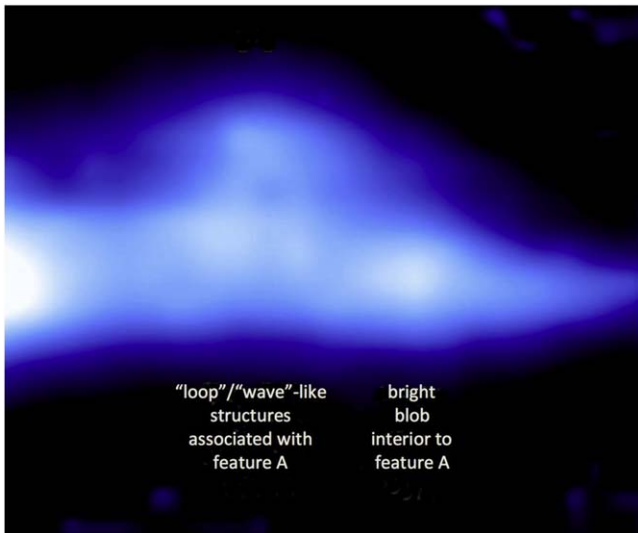


**Figure 2.** Inner region of the southeast side of AU Mic’s disk, spanning stellocentric separations of  $0''.815$  (right edge; 7.29 au) to  $1''.881$  (left edge; 18.28 au), is shown. The data are plotted on a log stretch after  $1/r^2$  scaling. Both the “loop-like” nature of feature A noted in Figure 1 and a bright blob interior to this feature are apparent. As noted in Section 3.1, the loop-like structure is located at a projected stellocentric separation of 14.2 au from AU Mic, and has a projected width of 1.5 au and rises 2.3 au above the disk midplane.

### 3.2. TESS Photometry

AU Mic was observed at 2 minute cadence in Sector 1 (2018 July 25–August 22) by the *TESS* (Ricker et al. 2015). We find the data exhibit a 4.86 day periodicity arising from starspot-induced stellar activity, as seen in the phase-folded light curve shown in Figure 3. This best-fit periodicity is very similar to that derived from Lomb–Scargle fitting (4.875 days; Lomb 1976; Scargle 1982). Two large, persistent spot complexes are clearly visible from the phase-folded light curve for  $\sim 60\%$  and  $\sim 40\%$  of the rotational period of the star, respectively.

### 3.3. Starspot Modeling

Extracting robust information about the surface distribution of starspots and spot complexes from traditional spot modeling is often not possible as there exists a degeneracy between the stellar inclination and spot latitude (Walkowicz et al. 2013). One can break this degeneracy in special cases, such as transiting planetary systems (Morris et al. 2017) or systems where the evolution of multiple spots can place weak constraints on their location (Davenport et al. 2015). AU Mic is well known to have a spatially resolved, edge-on debris disk; hence, it represents another case where we have good confidence about the stellar inclination axis, assuming the disk’s rotational axis is co-aligned. This assumption is supported by Watson et al. (2011), who reported the inclination of the disk ( $90^\circ$ ) to be the same as stellar rotational axis ( $90_{-20}^{+0}$ ), and is consistent with the small level of mutual inclination between the disk and stellar rotational axis ( $|\Delta i| = 1_{-1}^{+7}$ ) found by Greaves et al. (2014). Even in debris disk systems that have resolved disks and directly imaged planets with evidence of mutual misalignment, such as beta Pic b, the amplitude of this misalignment is small ( $\sim 3^\circ$ ).

Walkowicz et al. (2013) showed that the fraction of time that spots are visible in a system whose stellar inclination is seen

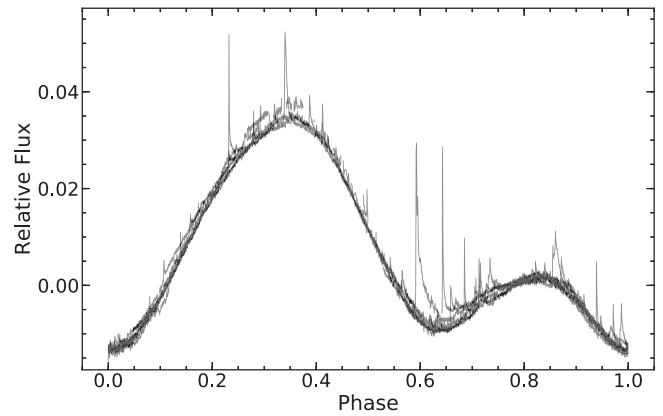


**Figure 3.** Phase-folded light curve of *TESS* observations of AU Mic exhibit periodic modulation arising from starspots.

edge-on, i.e.,  $i = 90^\circ$ , is a nearly uniform  $\sim 55\%$  of its rotational period, that rises to 60% near polar latitudes. Figure 3 demonstrates that the smaller amplitude spot complex in AU Mic’s phase-folded light curve persists for  $\sim 40\%$  of the star’s rotational period, which is not expected for standard edge-on systems (Walkowicz et al. 2013). Resolving this discrepancy demands relaxing the fundamental assumption of Walkowicz et al. (2013) that the rotational and magnetic field axes are co-aligned.

We utilize the starspot modeling software *STSP* developed by L. Hebb (2019, in preparation), as described in detail within Davenport et al. (2015), to model the *TESS* data. This software generates synthetic light curves for a star having a pre-defined number of static spots (or spot complexes), and computes spot properties (latitude, longitude, radius) from a  $\chi^2$  comparison between computed synthetic fluxes and observed fluxes using a Markov Chain Monte Carlo (MCMC) routine based on Foreman-Mackey et al. (2013). We used 50 parameter space walkers, with 20,000 steps in the MCMC chain.

We further explored the possibility of a mis-aligned  $B$  field in the system via a proxy, namely by varying the star’s “rotation axis” using a grid of MCMC runs from  $90^\circ$  (i.e., edge-on) to  $30^\circ$  in steps of  $15^\circ$ . Finding evidence of a preferred non-edge-on orientation via this modeling (given the evidence we have that the stellar rotational axis is co-aligned with the edge-on disk) serves as a proxy for the potential  $B$  field misalignment. Full 20,000 step MCMC explorations were independently run for each inclination, and the best (lowest  $\chi^2$ ) solution from the converged portion of the chains was considered. This grid found the rotation axis is weakly constrained from the starspot data alone, with the best model of  $i = 75^\circ$  being only slightly preferred ( $\Delta\chi^2 \sim 1$ ) over the edge-on solution. The *STSP* models more strongly rule out highly inclined scenarios of  $45^\circ$  and  $30^\circ$ . Thus, because we know the system inclination is *likely* edge-on from our spatially resolved imagery, the *STSP* results support the suggestion that the effective  $B$  field of AU Mic is misalignment with its rotational axis. Further quantifying the detailed topology of AU Mic’s  $B$  field via Zeeman–Doppler Imaging is strongly encouraged.

The resultant best-fit synthetic spot modeling light curve is shown in Figure 4 (red), along with the underlying *TESS* data (blue). The most likely relative latitude/longitude distribution of the two spot complexes in AU Mic are depicted in the bottom panels of Figure 4. We find the separation of the spots

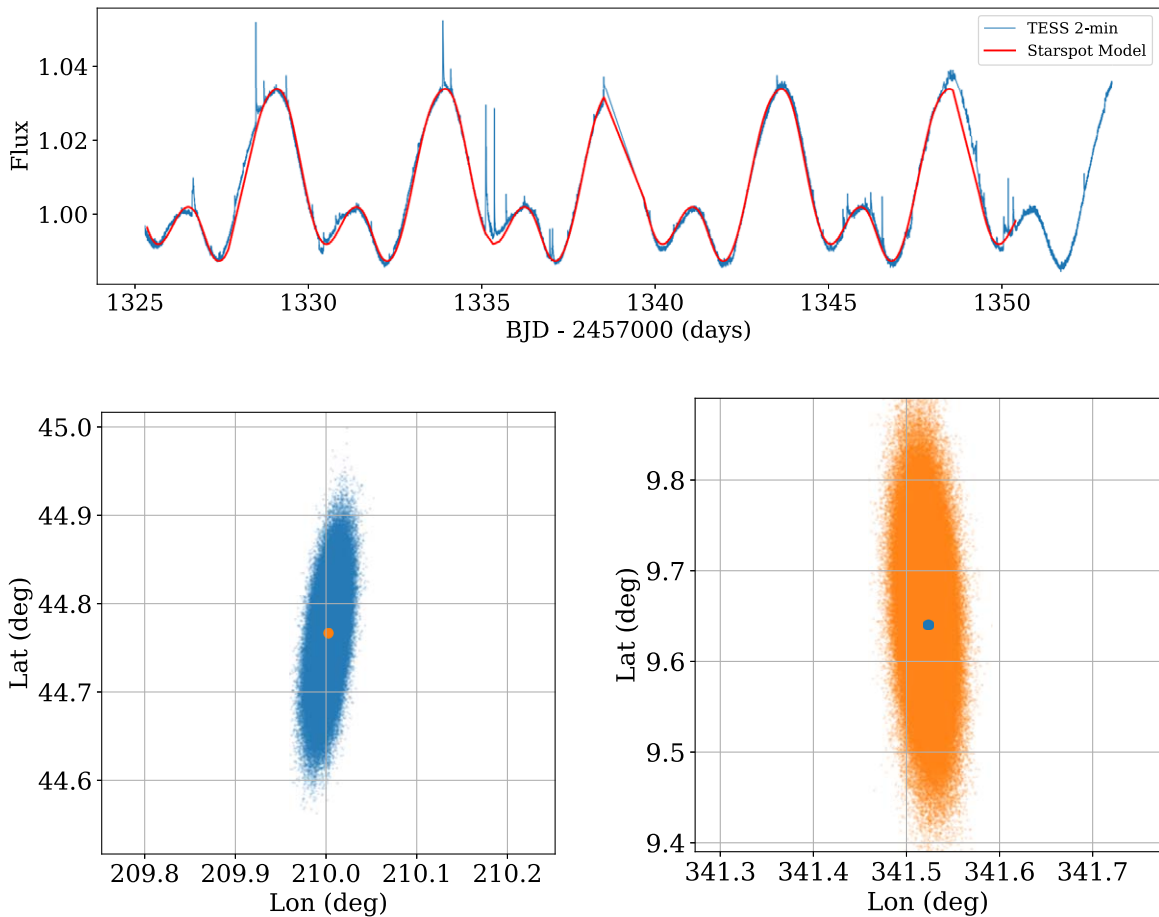


**Figure 4.** Top: *TESS* 2 minute light curve for AU Mic (blue) with sinusoidal starspot modulations and flares. Our best-fitting (lowest  $\chi^2$ ) stationary two starspot model from STSP is overlaid (red). Bottom: latitude and longitude locations of the two starspots from the converged portions of our affine-invariant MCMC chains, which trace the posterior probability distribution. The lowest  $\chi^2$  point is highlighted for each spot, which correlates to the model light curve above.

in latitude is significant, with one spot near the equator ( $\sim 9^\circ$ ) and the second spot at higher latitude ( $\sim 44^\circ$ ). The spots are separated by  $\sim 131^\circ$  in longitude.

## 4. Discussion

### 4.1. Origin of AU Mic’s Loop-like Disk Structure

Multi-epoch ground-based near-infrared coronagraphic imagery of AU Mic’s disk (Boccaletti et al. 2018), confirmed by higher photometric fidelity multi-epoch space-based optical coronagraphic imagery (Grady et al. 2019) has revealed evidence that the projected distribution of disk material evolves on both the projected vertical and radial directions. The detailed vertical evolution of these structures has been hard to quantify, given the sparse sampling of available high-fidelity observations. The vertical extension and evolution of these features necessarily requires the presence of non-radial forces. Chiang & Fung (2017) suggested, for example, that the star’s magnetized wind could exhibit a Lorentz force on grains and produce the vertical undulations observed in spatially resolved imagery if the polarity of the stellar magnetic field reverses periodically. The striking projected structure that our new *HST* imagery has revealed for feature A (Figures 1–2), i.e., a “loop-like” morphology, is suggestive that material is actively being lifted both above the midplane and back down toward the midplane on short timescales (i.e., significantly shorter than what could be caused by a change in the stellar magnetic field

polarity). One potential way to produce such morphologies on this timescale is if the disk is sculpted by a time-variable stellar wind. As discussed below, we suggest that a misalignment between the stellar  $B$  field and disk rotational axis (that is co-aligned with the stellar rotational axis) and/or a misalignment between the stellar rotational axis (co-aligned with the  $B$  field axis) and disk rotational axis could lead to the disk seeing different amounts of polar versus equatorial wind over time, producing morphological structure within the disk.

### 4.2. Evidence of Mis-aligned B Field and Potential Ramifications

We have shown in Section 3.3 that AU Mic’s edge-on debris disk allows a plausible way to break the spot latitude versus stellar inclination degeneracy and place constraints on the latitude of spots in the system (Figure 4). Walkowicz et al. (2013) aptly demonstrated that the fraction of time that spots are visible in a system whose stellar inclination is seen edge-on, i.e.,  $i = 90^\circ$ , is a nearly uniform  $\sim 55\%$  of its rotational period, that rises to 60% near polar latitudes. AU Mic’s phase-folded light curve (Figure 3) clearly violates this expectation, as its weaker amplitude spot is visible for  $\sim 40\%$  of its rotational phase. Because we know AU Mic’s stellar rotational axis with high confidence from its resolved disk (and studies that indicate minimal misalignment between the disk and stellar rotational axis, see, e.g., Watson et al. 2011; Greaves et al. 2014), this implies that it must have an offset magnetic field axis. Indeed,

our spot modeling in Section 3.3 supported this offset magnetic field interpretation. Offset magnetic field axes have been proposed in other dM systems like GJ 1243 (Davenport et al. 2015), and other astrophysical systems like magnetically confined disks surrounding massive B-type stars (Townsend et al. 2005; Townsend & Owocki 2005).

We consider the potential implications of AU Mic having a magnetic field axis that is offset from its rotational axis, and in particular the implications that this could have on its extended debris disk. Vidotto et al. (2014) found that non-axisymmetric surface magnetic fields can lead to more asymmetric mass fluxes. A common feature of the two leading dynamical models to explain the super-Keplerian motion of moving features in AU Mic’s disk is that both invoke the system’s stellar wind to disperse dust grains (Chiang & Fung 2017; Sezestre et al. 2017). We speculate that small grains in AU Mic’s disk could be sculpted by a time-dependent wind that could not only be enhanced by potentially large coronal mass ejections (Boccaletti et al. 2015) but also be influenced by the system having an offset  $B$  field axis. A potential analogy in the Sun are the interactions between the fast solar wind, that exits through coronal holes, and the slower solar wind, which creates stream interaction regions that co-rotate with the Sun (Richardson 2018). The effects of these solar interaction regions have been observed by the *Voyager* 1 and 2 and *Pioneer* 10 missions, including at stellocentric separations from the Sun ( $\sim 16$  au) similar to the current projected location of feature A in AU Mic (Burlaga et al. 1984; Burlaga 1988; Gazis et al. 1999; Richardson 2018). These time-dependent interaction regions create large-scale spiral density features that affect both the radial and vertical distribution of material in the Heliosphere. If analogous interaction regions exist around AU Mic, this could serve as one mechanism that could contribute to shaping the projected radial and vertical evolution of dust grains in AU Mic’s disk, as diagnosed by spatially resolved imagery. Although beyond the scope of this Letter, detailed dynamical modeling of such co-rotating interaction regions in the AU Mic system should be pursued. It could also be interesting to explore the magnetic field structure of other M-type debris disks that exhibit potential spiral-like structures, such as TWA 7 (Olofsson et al. 2018), to help assess whether they exhibit similarities to the AU Mic system.

### 4.3. Alternate Forms of Misalignment and Potential Ramifications

Our spot modeling (Section 3.3) and the associated interpretation of these results (Section 4.2) utilized previous research and observational properties of the system that indicated co-alignment of AU Mic’s stellar and disk rotational axes. We remark that if we relax this co-alignment prior, the observed phase-dependence of AU Mic’s spot coverage (two spot complexes visible for  $\sim 60\%$  and  $\sim 40\%$  of the rotational period, respectively) would demand misalignment between the edge-on disk and the stellar rotational axis. In such a scenario, our available data would not place constraints on the relative orientation of the  $B$  field. However, this misalignment would expose the disk to seeing different amounts of the equatorial versus more polar wind with each rotation of the star. We thus suggest that small grains in AU Mic’s disk could be similarly sculpted by such a time-dependent wind.

### 4.4. Using Edge-on Disks to Break Starspot Modeling Degeneracies

The advent of high-precision, high-cadence, long-duration photometric data sets from space-based missions like *Kepler* and *TESS* provide a unique opportunity to identify and characterize stellar activity arising from spot modulation across a large sample of low mass stars. We remark that our work with AU Mic reveals another unique way to break the degeneracy between stellar inclination and spot latitudes. Much like the special case of transiting planetary systems, whereby the presence of a transit allows one to deduce the stellar inclination angle with high precision (Morris et al. 2017), the subset of circumstellar disk systems that offer detailed inclination angle information (e.g., as measured from spatially resolved imaging for both edge-on, face-on, and intermediate inclination systems, or as inferred from photometric behavior like so-called “dipper” systems, which could suggest a likely near edge-on inclination; Cody et al. 2014) could provide another way to break key degeneracies in spot modeling. In particular, leveraging system inclinations from disk properties could enable one to map the detailed distribution of starspots and the prevalence of offset magnetic field axes from a large statistical sample of stars observed by *Kepler/TESS*.

We thank our referee for providing feedback that helped to improve both the clarity and content of this manuscript. This work was supported by a grant from STScI for GO-15219. We thank Suzanne Hawley, Jamie Lomax, Peter Plavchan, and Ben Tofflemire for helpful discussions of this work.

### ORCID iDs

John P. Wisniewski  <https://orcid.org/0000-0001-9209-1808>  
 Adam F. Kowalski  <https://orcid.org/0000-0001-7458-1176>  
 James R. A. Davenport  <https://orcid.org/0000-0002-0637-835X>  
 Glenn Schneider  <https://orcid.org/0000-0002-4511-5966>  
 Leslie Hebb  <https://orcid.org/0000-0003-1263-8637>  
 John H. Debes  <https://orcid.org/0000-0002-1783-8817>  
 Andras Gaspar  <https://orcid.org/0000-0001-8612-3236>  
 Dean C. Hines  <https://orcid.org/0000-0003-4653-6161>  
 Julien Milli  <https://orcid.org/0000-0001-9325-2511>

### References

- Augereau, J.-C., & Beust, H. 2006, *A&A*, 455, 987  
 Boccaletti, A., Sezestre, E., Lagrange, A.-M., et al. 2018, *A&A*, 614, A52  
 Boccaletti, A., Thalmann, C., Lagrange, A.-M., et al. 2015, *Natur*, 526, 230  
 Burlaga, L. F. 1988, *JGR*, 93, 4103  
 Burlaga, L. F., McDonald, F. B., Ness, N. F., et al. 1984, *JGR*, 89, 6579  
 Chiang, E., & Fung, J. 2017, *ApJ*, 848, 4  
 Cody, A. M., Stauffer, J., Baglin, A., et al. 2014, *AJ*, 147, 82  
 Daley, C., Hughes, A. M., Carter, E. S., et al. 2019, *ApJ*, 875, 87  
 Davenport, J. R. A., Hebb, L., & Hawley, S. L. 2015, *ApJ*, 806, 212  
 Fitzgerald, M. P., Kalas, P. G., Duchêne, G., Pinte, C., & Graham, J. R. 2007, *ApJ*, 670, 536  
 Foreman-Mackey, D., Hogg, D. W., Lang, D., & Goodman, J. 2013, *PASP*, 125, 306  
 Gaia Collaboration, Brown, A. G. A., Vallenari, A., et al. 2018, *A&A*, 616, A1  
 Gazis, P. R., McDonald, F. B., Burger, R. A., et al. 1999, *SSRv*, 89, 269  
 Grady, C. A., Wisniewski, J. P., Schneider, G., et al. 2019, APJL, submitted  
 Graham, J. R., Kalas, P. G., & Matthews, B. C. 2007, *ApJ*, 654, 595  
 Greaves, J. S., Kennedy, G. M., Thureau, N., et al. 2014, *MNRAS*, 438, L31  
 Hebb, L., Petro, L., Ford, H. C., et al. 2007, *MNRAS*, 379, 63  
 Kalas, P., Liu, M. C., & Matthews, B. C. 2004, *Sci*, 303, 1990  
 Krist, J. E., Ardila, D. R., Golimowski, D. A., et al. 2005, *AJ*, 129, 1008  
 Lellouch, E., Santos-Sanz, P., Lacerda, P., et al. 2013, *A&A*, 557, A60

- Liu, M. C. 2004, *Sci*, 305, 1442
- Lomax, J. R., Wisniewski, J. P., Roberge, A., et al. 2018, *AJ*, 155, 62
- Lomb, N. R. 1976, *Ap&SS*, 39, 447
- MacGregor, M. A., Wilner, D. J., Rosenfeld, K. A., et al. 2013, *ApJL*, 762, L21
- Mamajek, E. E., & Bell, C. P. M. 2014, *MNRAS*, 445, 2169
- Matthews, B. C., Kennedy, G., Sibthorpe, B., et al. 2015, *ApJ*, 811, 100
- Metchev, S. A., Eisner, J. A., Hillenbrand, L. A., & Wolf, S. 2005, *ApJ*, 622, 451
- Morris, B. M., Hebb, L., Davenport, J. R. A., Rohn, G., & Hawley, S. L. 2017, *ApJ*, 846, 99
- Olofsson, J., van Holstein, R. G., Boccaletti, A., et al. 2018, *A&A*, 617, A109
- Plavchan, P., Afanasev, D., Gilster, P., et al. 2019, *Natur*, submitted
- Richardson, I. G. 2018, *LRSP*, 15, 1
- Ricker, G. R., Winn, J. N., Vanderspek, R., et al. 2015, *JATIS*, 1, 014003
- Roberge, A., Weinberger, A. J., Redfield, S., & Feldman, P. D. 2005, *ApJL*, 626, L105
- Scargle, J. D. 1982, *ApJ*, 263, 835
- Schneider, G., Debes, J. H., Grady, C. A., et al. 2018, *AJ*, 155, 77
- Schneider, G., Grady, C. A., Hines, D. C., et al. 2014, *AJ*, 148, 59
- Schüppler, C., Löhne, T., Krivov, A. V., et al. 2015, *A&A*, 581, A97
- Sezestre, É., Augereau, J.-C., Boccaletti, A., & Thébault, P. 2017, *A&A*, 607, A65
- Stobie, E., & Ferro, A. 2006, in ASP Conf. Ser. 351, *Astronomical Data Analysis Software and Systems XV*, ed. C. Gabriel et al. (San Francisco, CA: ASP), 540
- Strubbe, L. E., & Chiang, E. I. 2006, *ApJ*, 648, 652
- Townsend, R. H. D., & Owocki, S. P. 2005, *MNRAS*, 357, 251
- Townsend, R. H. D., Owocki, S. P., & Groote, D. 2005, *ApJL*, 630, L81
- Vidotto, A. A., Jardine, M., Morin, J., et al. 2014, *MNRAS*, 438, 1162
- Walkowicz, L. M., Basri, G., & Valenti, J. A. 2013, *ApJS*, 205, 17
- Wang, J. J., Graham, J. R., Pueyo, L., et al. 2015, *ApJL*, 811, L19
- Watson, C. A., Littlefair, S. P., Diamond, C., et al. 2011, *MNRAS*, 413, L71
- Wood, B. E., Redfield, S., Linsky, J. L., Müller, H.-R., & Zank, G. P. 2005, *ApJS*, 159, 118